Check for updates

Theoretical prediction of corrosion inhibition by ionic liquid derivatives: a DFT and molecular dynamics approach†

Aymane Omari Alaoui,[a] Walid Elfalleh, [b] Belkheir Hammouti,[c] Abderrahim Titi,[d] Mouslim Messali,[e] Savas Kaya,[f] Brahim EL IBrahimi [gh] and Fadoua El-Hajjaji [*a]

Ionic liquids (ILs) have recently attracted significant attention in many domains, particularly as potential corrosion inhibitors owing to their outstanding properties, including low vapor pressure, high thermal and chemical stability, and the ability to be tailored for specific applications. Their effectiveness results mainly from their ability to strongly interact with metal surfaces, often *via* electrostatic and chemical interactions, thereby forming a protective barrier against corrosion. This study investigated three ionic liquids (ILs), namely, 3-(5-ethoxy-5-oxopentyl)-1-phenethyl-1*H*-imidazol-3-ium bromide ([5E5O-Imid] Br), 3-(6-ethoxy-6-oxohexyl)-1-phenethyl-1*H*-imidazol-3-ium bromide ([6E6O-Imid] Br), and 3-(4-acetoxybutyl)-1-phenethyl-1*H*-imidazol-3-ium bromide ([4AB-Imid] Br). This study aimed to assess the ILs' ability and efficiency to prevent mineral corrosion to understand the underlying mechanisms, as well as to identify the appropriate materials and timing prior to their experimental application. Density functional theory (DFT) was used to predict the electronic properties and reactivity of the molecules under investigation. Furthermore, molecular dynamics (MD) simulations were used to model the atomic−scale interactions between the ILs and metallic surfaces, offering in-depth insights into the adsorption mechanisms and interactions responsible for corrosion inhibitions.

1. Introduction

The search for effective methods to inhibit corrosion has led to the development of various strategies, wherein corrosion inhibitors play a key role. Among various corrosion inhibitors, ionic liquids (ILs), which are molten salts at ambient temperature, have attracted growing interest because of their distinctive properties, including low vapor pressure, excellent thermal

ªSystems Engineering, Modeling and Analysis Laboratory, Faculty of Sciences Dhar El Mahraz, Sidi Mohamed Ben Abdellah University, BP 1796 Atlas, Fez 30000, Morocco. E-mail: fadoua.elhajjaji@usmba.ac.ma

ᵇDepartment of Biology, College of Science, Imam Mohammad Ibn Saud Islamic University (IMSIU), Riyadh, 11623, Saudi Arabia

ᶜEuromed University of Fes, UEMF, Fes, Morocco

ᵈEngineering Laboratory of Organometallic, Molecular Materials and Environment (LIMOME), Faculty of Sciences Dhar El Mahraz, Sidi Mohamed Ben Abdellah University, BP 1796 Atlas, Fez 30000, Morocco

ᵉDepartment of Chemistry, College of Science, Imam Mohammad Ibn Saud Islamic University (IMSIU), PO Box 90950, Riyadh 11623, Saudi Arabia

ᶠSivas Cumhuriyet University, Health Services Vocational School, Department of Pharmacy, Sivas, 58140, Turkey

ᵍFaculty of Applied Sciences, Department of Applied Chemistry, IBNOU ZOHR University, 86153 Aït Melloul, Morocco

ʰLaboratory of Organic Chemistry and Physical Chemistry of Sciences, IBNOU ZOHR University, 80000 Agadir, Morocco

† Electronic supplementary information (ESI) available. See DOI: https://doi.org/10.1039/d5ra01097g

stability, and the ability to dissolve a broad spectrum of chemical substances. These features make ILs especially effective at preventing corrosion by forming a stable protective layer at the metal–electrolyte interface.[1–4]

Despite the high potential of ILs as corrosion inhibitors,[5–10] a more thorough understanding of the atomic and electronic mechanisms underlying their effectiveness is still required to optimize their application in real-world scenarios.[11]

Predicting the results of electrochemical corrosion-inhibition tests is crucial for optimizing material protection, reducing costs, and saving time in developing effective solutions. Such predictions allow a rapid identification of the most efficient inhibitors, helping adjust their concentration and tailor treatments to specific conditions of use while minimizing the number of physical tests required. This approach also helps estimate the long-term durability of materials and provide guidance on how to extend their lifespan and better plan maintenance. Furthermore, it facilitates the design of new materials and inhibitors, ensures compliance with environmental and safety regulations, and contribute to a deeper understanding of corrosion mechanisms. Thus, predicting electrochemical test results is an essential tool for developing more economical, sustainable, and industry-specific solutions.

Significant progress has been made in corrosion-inhibition technologies using IL structures in recent years. However, to date, most studies have focused on the efficiency of these

systems only under experimental conditions. The novelty of our work lies in the application of imidazolium-based ILs in theoretical studies based on density functional theory (DFT) and molecular dynamics (MD). These studies were conducted to explore the atomic–scale interactions between ILs and metallic surfaces and to predict the behavior of these systems under various conditions. Furthermore, this study proposes a combined approach using DFT and MD simulations to examine the corrosion-inhibition mechanisms of three derivatives of ILs: 3-(5-ethoxy-5-oxopentyl)-1-phenethyl-1*H*-imidazol-3-ium bromide ([5E5O-Imid] Br), 3-(6-ethoxy-6-oxohexyl)-1-phenethyl-1*H*-imidazol-3-ium bromide TA11 ([6E6O-Imid] Br) and 3-(4-acetoxybutyl)-1-phenethyl-1*H*-imidazol-3-ium bromide ([4AB-Imid] Br).[12] We aimed to predict the experimental test outcomes by providing a detailed description of the metallic surface structure in the presence of the ILs, their atomic–level interactions,[13] and the associated thermodynamic and kinetic processes. The theoretical results obtained will not only enhance the understanding of interactions between ILs and metals but also guide the design of more effective ILs for corrosion inhibition.[14] Thus, this study represents a crucial step toward the development of innovative solutions for combating corrosion while strengthening the theoretical foundations for the application of ILs as a means of protecting metallic materials from degradation.[15]

2. Experimental section

2.1. Chemical synthesis and characterization

The alkyl halides ethyl 5-bromopentanoate, ethyl 6-bromohexanoate, and/or 4-bromobutyl acetate (1.1 eq) were introduced into a solution of 1-phenethyl-1*H*-imidazol (1 eq) in toluene. The mixture was then irradiated for 20 min in a sealed vessel at 80 °C using a CEM microwave. The reaction was considered complete when the initially clear, homogeneous mixture of 1-

phenethyl-1*H*-imidazol and alkyl halide in toluene transformed into an oily phase.[16] The product was extracted with ethyl acetate. Subsequently, the IL was dried under reduced pressure. The ILs examined are illustrated in Fig. 1.

2.2. Theoretical details

It is well-known that conceptual density functional theory (CDFT)[17] is a useful tool for analyzing the global and local chemical reactivities of molecules with the help of chemical concepts like the chemical potential (μ), electronegativity (χ), hardness (η), softness (σ), electrophilicity (ω) and nucleophilicity (ε). In the theory, chemical potential and hardness are defined as first and second derivatives concerning the number of electrons (N) of total electronic energy (E) at a constant external potential. While electronegativity is defined as the negative of the chemical potential, softness is presented as the multiplicative inverse of the hardness. Considering the finite differences approach, Parr and Pearson presented the following equations based on the ground-state ionization energy (I) and electron affinities (A) of chemical species to calculate the aforementioned quantum chemical parameters.[17]

$$\mu = -\chi = \left[\frac{\partial E}{\partial N}\right]_{\nu(r)} = -\left(\frac{I + A}{2}\right) \quad (1)$$

$$\eta = \frac{1}{2}\left[\frac{\partial^2 E}{\partial N^2}\right]_{\nu(r)} = \frac{I - A}{2} \quad (2)$$

$$\sigma = 1/\eta \quad (3)$$

Considering the Koopmans[18] theorem introduced in the 1930s, the negative values of HOMO and LUMO are approximately equal to the ionization energy and electron affinity in the ground state, whereby the formulas given above turn into the following equations:
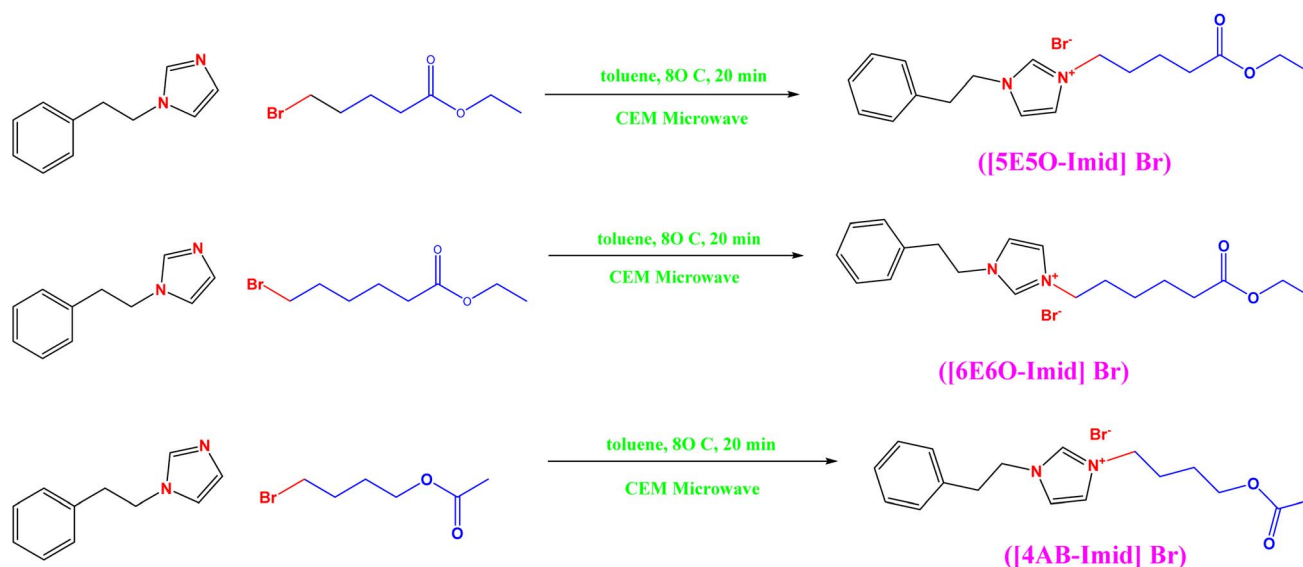

Fig. 1 Synthesis reaction of ILs bromide.

$$\mu = -\chi = \frac{E_{HOMO} + E_{LUMO}}{2} \tag{4}$$

$$\eta = \frac{E_{LUMO} - E_{HOMO}}{2} \tag{5}$$

$$\sigma = \frac{1}{E_{LUMO} - E_{HOMO}} \tag{6}$$

The electrophilicity index (ω) formulated by Parr, Szentpaly, and Liu[19] provides important evidence of the electrophilic powers of molecular systems. It is based on the electronegativity and hardness values of the related system. Chattaraj presented the nucleophilicity index (ε) as the multiplicative inverse of the electrophilicity index.

$$\omega = \chi^2/2\eta = \mu^2/2\eta \tag{7}$$

$$\varepsilon = 1/\omega \tag{8}$$

in corrosion studies, it is important to predict the electron-donating ($\omega-$) and electron-accepting ($\omega+$) powers of the related compounds. Gazquez and coworkers[20] suggested that $\omega-$ and $\omega+$ depend on the ionization energy and electron affinity of the system:

$$\omega^+ = (I + 3A)^2/(16(I - A)) \tag{9}$$

$$\omega^- = (3I + A)^2/(16(I - A)) \tag{10}$$

The fraction of electrons transferred and metal–inhibitor interaction energy equations derived from electronegativity equalization and hardness equalization principles are given below:[21]

$$\Delta N = \frac{\phi_M - \chi_{inh}}{2(\eta_M + \eta_{inh})} \tag{11}$$

$$\Delta\psi = -\frac{(\phi_M - \chi_{inh})^2}{4(\eta_M + \eta_{inh})} \tag{12}$$

It is well-known that the fraction of electrons transferred (ΔN) and the metal–inhibitor interaction energy ($\Delta\psi$) provide significant insights into the corrosion-inhibition performances of molecules and the power of the interaction between the inhibitor and metal surface. Here, the variables are defined as follows:

χ_{inh}: the electronegativity of the inhibitor, η_M: the hardness of the metal surface, and η_{inh}: the hardness of the inhibitor. It should be noted that $\eta_M = 0$ assumes that for a metallic bulk I = A, and the work function value for the Fe (110) surface is 4.82 eV.

All B3LYP computations at the 6311 G (df, pd) basis set were performed utilizing the G09W package. The C-PCM (conducted polarized continuum model) solvent model employed the water-phase simulations. The pictorial representations were prepared using the Gaussview 6.0.16 package.

MD simulation studies can provide important insights into the interactions between inhibitor molecules and metal surfaces. To get further insights at the atomic scale, molecular dynamics (MD) calculations were carried out under solvation conditions using a solution composition of 100 H_2O + 3 Cl^- + $3H_3O^+$ + Br^-. The simulation was performed in a box with dimensions of 25 A × 25 A × 94 A, comprising 8 Fe (110) layers with 11 × 11 Fe atoms per face and 80 A as a vacuum region. The temperature of the studied systems was fixed at 298 K using the Andersen thermostat. For the simulation time, 250 ps was selected with 1 fs as the time step. All calculations were conducted under periodic boundary conditions and employing COMPASS as a force field. Ewald and atom-based summation methods were used to compute the electrostatic and van der Waals interactions, respectively. Eqn (13) was used to calculate the adsorption energy regarding the interaction process.[22]

$$E_{ads} = E_{total} - (E_{solution+metal} + E_{inhibitor}) \tag{13}$$

in this equation, E_{total} stands for the total energy of the system. $E_{solution+metal}$ represents the total energy of the system without any inhibitor molecule, and $E_{inhibitor}$ is the energy of the inhibitor molecule.

## 3. Results and discussion

3.1. Characterization of the ILs

3.1.1. 3-(5-Ethoxy-5-oxopentyl)-1-phenethyl-1*H*-imidazol-3-ium bromide ([5E5O-Imid] Br). FT-IR, cm^{-1}: 747 (C–H, CH_2), 1030 (C–O), 1154 (C–N), 1561 (C=N), 1725 (C=O), and 2910 and 3090 (Ar–H). 1H NMR (400 MHz, CDCl$_3$): δ_H = 1.18 (3H, CH_3), 1.48 (quint, 2H, CH_2), 1.85 (quint, 2H, CH_2), 2.29 (t, 2H, CH_2), 3.19 (t, 2H, CH_2), 4.04 (qd, 2H, CH_3), 4.24 (t, 2H, CH_2), 7.30–7.57 (d, 2H, Ar–H), 7.05–7.47 (m, 5H, Ar–H), and 9.97 (s, 1H, Ar–H); 13C NMR (100 MHz, CDCl$_3$): δ_C = 14.2 (CH_3), 21.6 (CH_2), 29.9 (CH_2), 33.1 (CH_2), 36.4 (CH_2), 49.56 (CH_2), 51.0 (CH_2), 60.5 (CH_2), 121.9 (CH), 122.5 (CH), 127.3 (CH), 128.8 (CH), 128.9 (CH), 135.8 (C), 136.5 (CH), and 172.9 (CO); found: C, 56.81, H, 6.55, N, 7.42%. Calcd. for $C_{18}H_{25}BrN_2O_2$, C, 56.70, H, 6.61, N, 7.35%.

3.1.2. 3-(6-Ethoxy-6-oxohexyl)-1-phenethyl-1*H*-imidazol-3-ium bromide TA11 ([6E6O-Imid] Br). FT-IR, cm^{-1}: 751 (C–H, CH_2), 1097 (C–O), 1154 (C–N), 1561 (C=N), 1725 (C=O), and 2910 and 3090 (Ar–H). 1H NMR (400 MHz, CDCl$_3$): δ_H = 1.15 (3H, CH_3), 1.18 (quint, 2H, CH_2), 1.53 (quint, 2H, CH_2), 1.76 (quint, 2H, CH_2), 2.19 (t, 2H, CH_2), 2.2 (t, 2H, CH_2), 3.12 (t, 2H, CH_2), 4.02 (qd, 2H, $CH3$), 4.17 (t, 2H, CH_2), 7.28–7.55 (d, 2H, Ar–H), 7.01–7.45 (m, 5H, Ar–H), and 9.91 (s, 1H, Ar–H); 13C NMR (100 MHz, CDCl$_3$): δ_C = 14.2 (CH_3), 23.9 (CH_2), 25.3 (CH_2), 29.8 (CH_2), 33.6 (CH_2), 36.3 (CH_2), 49.6 (CH_2), 50.9 (CH_2), 60.3 (CH_2), 121.9 (CH), 122.6 (CH), 127.3 (CH), 128.8 (CH), 128.9 (CH), 135.8 (C), 136.5 (CH), and 173.3 (CO); found: C, 57.80, H, 6.79, N, 7.15%. Calcd. for $C_{19}H_{27}BrN_2O_2$, C, 57.72, H, 6.88, N, 7.09%.

3.1.3. 3-(4-Acetoxybutyl)-1-phenethyl-1*H*-imidazol-3-ium bromide ([4AB-Imid] Br). FT-IR, cm^{-1}: 747 (C–H, CH_2), 1154 (C–N), 1238 (C–O), 1561 (C=N), 1725 (C=O), and 2910 and 3080 (Ar–H). 1H NMR (400 MHz, CDCl$_3$): δ_H = 1.16 (quint, 2H, CH_2),
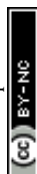
1.84 (3H, CH3), 2.17 (quint, 2H, CH2), 3.17 (t, 2H, CH$_2$), 4.00 (t, 2H, CH$_2$), 4.17 (qd, 2H, CH$_3$), 4.56 (t, 2H, CH$_2$), 7.15–7.43 (d, 2H, Ar–H), 7.09–7.34 (m, 5H, Ar–H), 9.92 (s, 1H, Ar–H); 13C NMR

(100 MHz, CDCl$_3$): δ_C = 20.9 (CH3), 25.1 (CH$_2$), 26.9 (CH$_2$), 36.3 (CH$_2$), 49.3 (CH2), 50.9 (CH$_2$), 63.2 (CH$_2$), 122.1 (CH), 122.6 (CH), 127.3 (CH), 128.8 (CH), 128.9 (CH), 135.8 (C), 136.5 (CH), and 171.1 (C); found: C, 55.66, H, 6.25, N, 7.70%. Calcd. for C$_{17}$H$_{23}$BrN$_2$O$_2$, C, 55.59, H, 6.31, N, 7.63%.

The ^{1}H NMR, ^{13}C NMR, and DEPT-135NMR spectra of the studied ILs are shown in Fig. 2.

3.2. Theoretical study

3.2.1. DFT study. FMO analysis provides significant information for evaluation of the corrosion-inhibition capability of potential molecular systems; whereby higher HOMO and lower LUMO energies imply the electron-donating and electron-accepting capabilities of a molecular system, respectively. The predicted corrosion-inhibition efficiency ranking in light of the calculated frontier orbital energies was [6E6O-Imid] Br > [5E5O-Imid] Br > [4AB-Imid] Br. Chemical hardness[23] represents the resistance against the electron cloud polarization of molecules. Two important electronic structure principles are proposed in the literature about the hardness concept. One of them is the famous hard and soft acid–base principle of Pearson, and the other is the maximum hardness principle,[24] which states that "there seems to be a rule of nature that molecules arrange themselves so as to be as hard as possible" and suggests that the hardness is a measure of stability. Ghanty and Ghosh[25] reported a remarkable correlation between softness and polarizability, stating that softness is proportional to the cube root of polarizability. Chemical compounds with high polarizability values give electrons easily to metal surfaces and thus act as effective corrosion inhibitors. The minimum polarizability principle[26] states that in a stable state, polarizability is minimized. Within the framework of calculated polarizability values, the inhibition efficiency order of the molecules studied here can be given as [6E6O-Imid] Br > [5E5O-Imid] Br > [4AB-Imid] Br. Electronegativity[27] measures the electron-withdrawal powers of chemical species, while electrophilicity reflects the electron-accepting tendency of electron-rich species of chemical species. It should be noted that an effective corrosion inhibitor should have low electronegativity and low electrophilicity values. If so, with the help of the calculated electronegativity and electrophilicity index values, one can write the corrosion-inhibition efficiency order of our studied molecules as: [6E6O-Imid] Br > [5E5O-Imid] Br > [4AB-Imid] Br (Table 1). The principles of the electron-accepting power and electron-donating power imparted to science by Gazquez and coworkers can help corrosion scientists to predict molecules' electron-donating and electron-accepting capabilities. Here, the electron-accepting power value of the [6E6O-Imid] Br molecule was lower than that of the other molecules. For that reason, the mentioned molecule had a higher corrosion-inhibition performance compared to the others. The fraction of electrons transferred from the inhibitor molecule to the metal surface is an essential indicator of the corrosion-inhibition efficiencies of molecules. For $\Delta N > 0$, the direction of electron transfer is from the inhibitor to the metal surface. Higher values of ΔN belong to effective corrosion inhibitors. On the other hand, the metal–inhibitor interaction
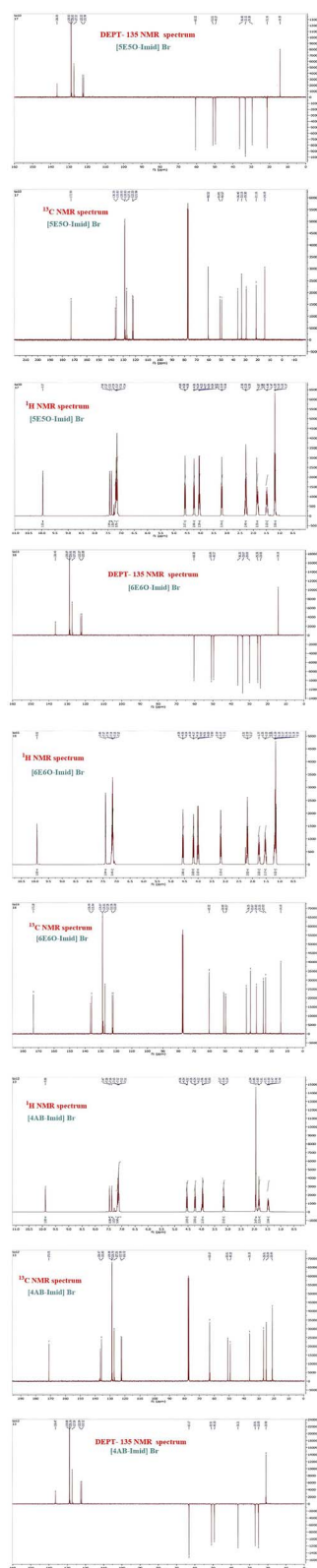

**Fig. 2** ^{1}H NMR, ^{13}C NMR, and DEPT-135 NMR spectra of the studied ILs.

Table 1 Quantum chemical parameters of ionic liquid (IL) compounds at the B3LYP/6-311G (df,pd) level

	Gas			Water		
	TA10	TA11	TA12	TA10	TA11	TA12
HOMO($_{-I}$)	−5.0009	−4.9683	−5.1963	−6.3528	−6.3544	−6.3577
LUMO (-A)	−1.2174	−1.1080	−1.3791	−0.9821	−0.9622	−0.9823
ΔE (L–H)	3.7835	3.8602	3.8172	5.3707	5.3922	5.3753
μ	−3.1092	−3.0382	−3.2877	−3.6674	−3.6583	−3.6700
η	1.8917	1.9301	1.9086	2.6854	2.6961	2.6877
ω	2.5551	2.3912	2.8316	2.5043	2.4819	2.5057
ω^+	1.2369	1.1133	1.4263	1.0063	0.9898	1.0066
ω^-	4.3461	4.1515	4.7140	4.6737	4.6481	4.6766
ΔN	0.4522	0.4616	0.4014	0.2146	0.2154	0.2139
$\Delta \Psi$	−0.3868	−0.4112	−0.3076	−0.1237	−0.1251	−0.1230
D (Debye)	10.7552	10.4880	12.7259	20.2189	18.7976	22.0674
α (au)	243.5890	257.1933	231.3780	295.8327	311.1317	280.8333
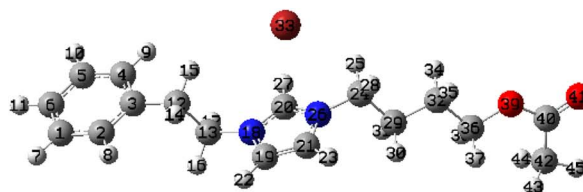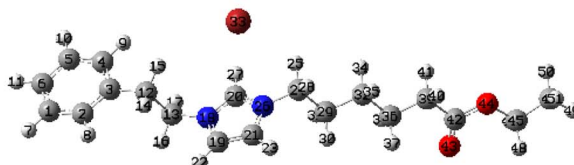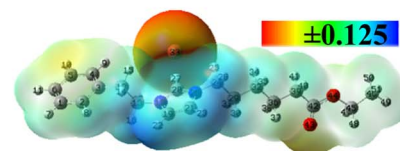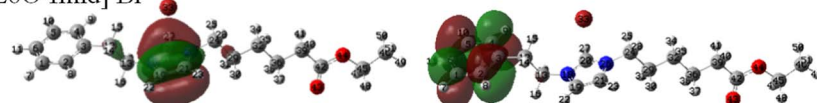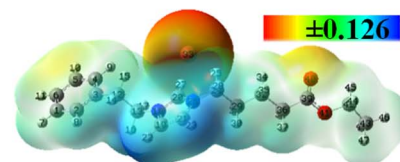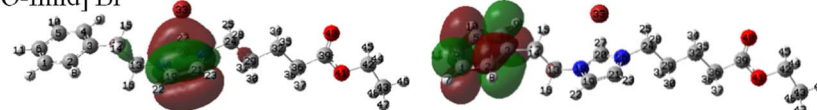
Fig. 3 Optimized structures, HOMO and LUMO (iso value: 0.02), and MEP (iso value: 0.0004) plots of the IL compounds at the B3LYP/6-311G (df,pd) level in the water phase.

energy also gives valuable information about the corrosion-inhibition performances of inhibitor molecules. As the metal–inhibitor interaction energy becomes negative, the corrosion-inhibition efficiency increases. Based on the calculated ΔN and $\Delta \psi$ values presented in Table 1, the 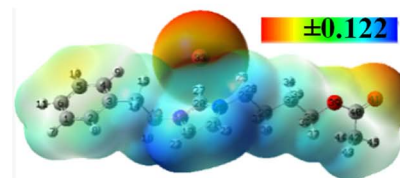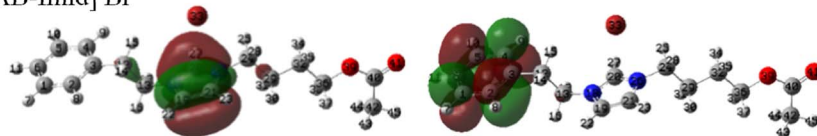corrosion-inhibition efficiency ranking of the studied molecules can be given as: [6E6O-Imid] Br > [5E5O-Imid] Br > [4AB-Imid] Br. Here, it should be stated that the reactivity tendency of the compounds slightly differed, which means that the additional –CH₂ group or -O-C═O group position on the main chain of the compounds had a negligible effect on their chemical reactivity behavior (Fig. 3). The nucleophilic and electrophilic attack regions of all the compounds were predicted to be similar to each other; particularly, there was no calculated HOMO or LUMO density on the main –CH₂ chain and –O–C═O (ester) groups. HOMO, as an indicator of the nucleophilic attack site, was extended on the imidazol ring. In contrast, LUMO, a sign of the electrophilic attack site, was spread over the phenyl group. Moreover, MEP graphs exhibited possible electronic attack regions for the molecular system. In the MEP plots, electron charge density is given by the color scale depending on the electrostatic potential on the molecular surface: red denotes the electron-rich region having the most negative electrostatic potential, and blue expresses the electron-poor region having the most positive electrostatic potential.[20] From Fig. 3, it could be seen that mainly Br⁻ ions and, partially, oxygen atoms were determined as the electron-rich sites for all the compounds. Furthermore,

the –CH₂ groups neighboring the nitrogen atoms of the imidazol ring were defined as partially electron-poor sites as indicated by their moderate size blue color.

Elhachmia et al.[28] utilized the same study of two molecules ([OB-IM+, Cl⁻], [OE-IM+, Cl⁻]), which have similar structures to our inhibitors but differ in terms of their alkyl chain length. The results from the DFT calculations in their paper are generally comparable to our study. This research demonstrated the ability to donate energy, and showed that the ΔN and $\Delta \psi$ values increased as the alkyl chain length increased. Therefore, the predicted ranking for the corrosion-inhibition efficiency based on the calculated properties was reported to be: [OB-IM+, Cl⁻] > [OE-IM+, Cl⁻]. This aligned with the experimental results, which showed values of 96.3 and 95.9 for [OB-IM+, Cl⁻] and [OE-IM+, Cl⁻], respectively. This is also related to what we refer to in our study, a means of providing a theoretical prediction of the experimental results one could expect from the products to be tested.

3.2.2. Molecular dynamic calculations. Molecular dynamics simulations can provide valuable insights into the adsorption behavior of inhibitor molecules. Generally, adsorption and binding energies, critical indicators of corrosion-inhibition efficiency, that show more negative values indicate better performance. Fig. 4 illustrates the most stable adsorption modes for the examined inhibitors in our study, with the results aligning well with the experimental data, while the adsorption energies are listed in Table 2.

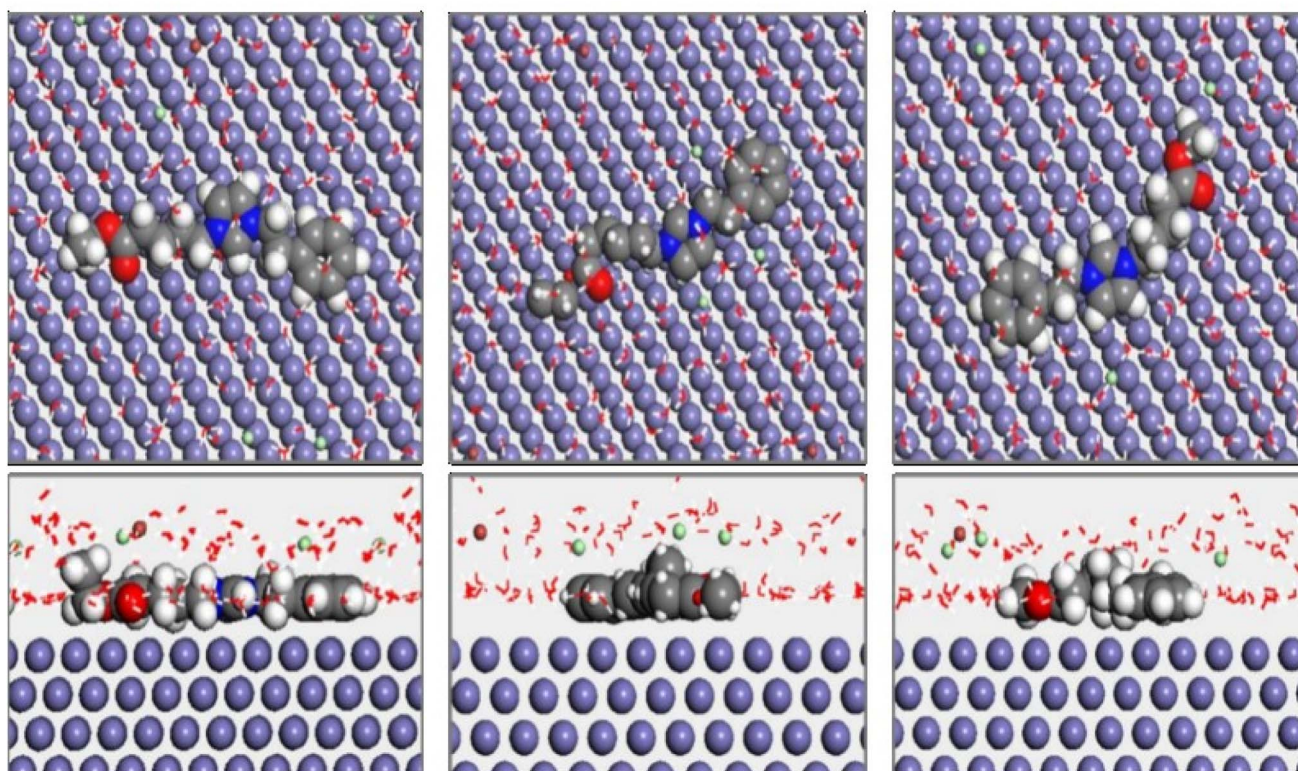**[5E5O-Imid] Br @ Fe110 [6E6O-Imid] Br @ Fe110 [4AB-Imid] Br @ Fe110**

Fig. 4 Top and side views of the equilibrium adsorption geometries of the examined inhibitors on the Fe (110) surface after the MD process.

Table 2 Adsorption and binding energies (Kcal mol^{-1}) of the investigated inhibitors

Molecules	E_{ads}	$E_{Binding}$
[5E5O-Imid] Br	−195.970	195.970
[6E6O-Imid] Br	−230.106	230.106
[4AB-Imid] Br	−191.418	191.418

Table 2 presents the adsorption energy values regarding the interactions between the studied inhibitor molecules and the Fe (110) metal surface. It is important to note that binding energy is the negative of adsorption energy. The reason for selecting the Fe (110) surface in the calculations was its stable structure. It is well-known that the MD simulation approach is an essential tool for obtaining the most stable adsorption mode of metal–inhibitor interactions. Fig. 4 depicts the equilibrium adsorption geometries of the examined inhibitors on the Fe (110) surface after the MD process. Considering the calculated adsorption and binding energies, the corrosion-inhibition performances of the molecules can be easily compared. Notably, more negative adsorption energy values indicate excellent and effective corrosion inhibitors.[29,30] Here, the calculated adsorption energy values regarding the interactions with the Fe (110) surface of [6E6O-Imid] Br, [5E5O-Imid] Br, and [4AB-Imid] Br were 195.970, −230.106, and −191.418 kcal mol^{-1}, respectively. This is what was also found in the inhibitors [OE$^-$IM$^+$, Cl$^-$] and [OB-IM+, Cl$^-$],[28] which gave high negative adsorption energy values with the surface of the Fe (110) metal, which was appropriate for experimental values that indicated a high corrosion-inhibition efficacy. We can see that our inhibitors had slightly higher adsorption energy values compared with [OE-IM+, Cl$^-$] and [OB-IM+, Cl$^-$]; hence, we can say that our compounds are more stable and therefore can have a larger inhibitor efficiency. Thus, finally, it can be noted that the results of DFT calculations and MDS studies could be good predictions for conducting future experiments.

4. Conclusion

The inhibition mechanisms of ILs, namely, [5E5O-Imid] Br, [6E6O-Imid] Br, and 3 [4AB-Imid] Br, were detailed, highlighting the atomic and electronic interactions underlying their effectiveness. The analysis of their adsorption energies and thermodynamic and kinetic properties revealed the significant potential of these ILs in preventing corrosion. Theoretical results can guide future experimental studies aimed at validating the predictions and identifying the optimal conditions to maximize the effectiveness of ILs as corrosion inhibitors.

In conclusion, this study provides a solid foundation for the development of innovative solutions against corrosion while emphasizing the importance of theoretical approaches in designing new, more effective materials and inhibitors.

Data availability

Data will be made available upon request by the corresponding author.

Conflicts of interest

The authors declare no conflicts of interest.

Acknowledgements

References

1 F. El-Hajjaji, R. Salim, E. Ech-chihbi, A. Titi, M. Messali, S. Kaya, B. El Ibrahimi and M. Taleb, New imidazolium ionic liquids as ecofriendly corrosion inhibitors for mild steel in hydrochloric acid (1 M): experimental and theoretical approach, *J. Taiwan Inst. Chem. Eng.*, 2021, **123**, 346–362.

2 H. Elmsellem, N. Basbas, A. Chetouani, A. Aouniti, S. Radi, M. Messali and B. Hammouti, Quantum Chemical Studies and Corrosion Inhibitive Properties of Mild Steel by Some Pyridine Derivatives in 1 N HCl Solution, *Port. Electrochim. Acta*, 2014, **32**(2), 77–108.

3 A. Ait Mansour, A. Elmoutaouakil Ala Allah, H. Lgaz, M. Messali, H. Lee, L. Bazzi, R. Salghi, Y. Ramli and B. Hammouti, Evaluation of N80 Carbon Steel Corrosion in 15 wt.% HCl Using Isatin-hydrazones: A Comprehensive Approach with Chemical, Electrochemical Techniques, and DFTB Calculations, *J. Mol. Struct.*, 2025, **1321**, 139910.

4 S. Gurjar, S. K. Sharma, A. Sharma and S. Ratnani, Performance of imidazolium based ionic liquids as corrosion inhibitors in acidic medium: A review, *Appl. Surf. Sci. Adv.*, 2021, **6**, 100170.

5 M. Bouklah, B. Hammouti, M. Benkaddour and T. Benhadda, Thiophene derivatives as effective inhibitors for the corrosion of steel in 0.5 m H$_2$SO$_4$, *J. Appl. Electrochem.*, 2005, **35**, 1095–1101.

6 D. S. Chauhan, F. El-Hajjaji and M. A. Quraishi, *Chapter 18 - Heterocyclic Ionic Liquids as Environmentally Benign Corrosion Inhibitors: Recent Advances and Future Perspectives*, Elsevier, 2022, pp. 279–294.

7 I. B. Obot, I. B. Onyeachu, S. A. Umoren, M. A. Quraishi, A. A. Sorour, T. Chen, N. Aljeaban and Q. Wang, High temperature sweet corrosion and inhibition in the oil and gas industry: progress, challenges and future perspectives, *J. Pet. Sci. Eng.*, 2020, **185**, 106469.

8 C. Verma, E. E. Ebenso and M. A. Quraishi, Ionic liquids as green and sustainable corrosion inhibitors for metals and alloys: an overview, *J. Mol. Liq.*, 2017, **233**, 403–414.

9 M. Deetlefs, K. R. Seddon and M. Shara, Predicting physical properties of ionic liquids, *Phys. Chem. Chem. Phys.*, 2006, **8**(5), 642–649.

10 M. Zhang, R. Ettelaie, T. Yan, S. Zhang, F. Cheng, B. P. Binks and H. Yang, Ionic Liquid Droplet Microreactor for Catalysis Reactions Not at Equilibrium, *J. Am. Chem. Soc.*, 2017, **139**(48), 17387–17396.

11 D. K. Verma, Y. Dewangan, A. K. Singh, R. Mishra, M. A. Susan, R. Salim, M. Taleb, F. El Hajjaji and E. Berdimurodov, Ionic liquids as green and smart lubricant application: an overview, *Ionics*, 2022, **28**(11), 4923–4932.

12 A. A. Toledo Hijo, G. J. Maximo, M. C. Costa, E. A. Batista and A. J. Meirelles, Applications of ionic liquids in the food and bioproducts industries, *ACS Sustain. Chem. Eng.*, 2016, **4**(10), 5347–5369.

13 A. Nicosia, W. Gieparda, J. Foksowicz-Flaczyk, J. Walentowska, D. Wesołek, B. Vazquez, F. Prodi and F. Belosi, Air filtration and antimicrobial capabilities of electrospun PLA/PHB containing ionic liquid, *Sep. Purif. Technol.*, 2015, **154**, 154–160.

14 Q. Chu, J. Liang and J. Hao, Electrodeposition of zinc-cobalt alloys from choline chloride–urea ionic liquid, *Electrochim. Acta*, 2014, **115**, 499–503.

15 F. El-Hajjaji, M. Messali, M. V. Martínez de Yuso, E. Rodríguez-Castellón, S. Almutairi, T. J. Bandosz and M. Algarra, Effect of 1-(3-phenoxypropyl) pyridazin-1-ium bromide on steel corrosion inhibition in acidic medium, *J. Colloid Interface Sci.*, 2019, **541**, 418–424.

16 A. Titi, S. M. Almutairi, A. F. Alrefaei, S. Manoharadas, B. A. Alqurashy, P. k. Sahu, B. Hammouti, R. Touzani, M. Messali and I. Ali, *J. Mol. Liq.*, 2020, **315**, 113778.

17 F. El Hajjaji, R. Salim, M. Messali, B. Hammouti, D. Chauhan, S. Almutairi and M. Quraishi, Electrochemical Studies on New Pyridazinium Derivatives as Corrosion Inhibitors of Carbon Steel in Acidic Medium, *J. Bio- Tribo-Corros.*, 2019, **5**, 4.

18 E. Ech-chihbi, M. E. Belghiti, R. Salim, H. Oudda, M. Taleb, N. Benchat, B. Hammouti and F. El-Hajjaj, Experimental and computational studies on the inhibition performance of the organic compound "2-phenylimidazo [1,2-*a*]pyrimidine-3-carbaldehyde" against the corrosion of carbon steel in 1.0 HCl solution, *Surf. Interfac.*, 2017, **9**, 206–217.

19 A. Zarrouk, M. Messali, H. Zarrok, R. Salghi, A. A. Ali, B. Hammouti, S. S. Al-Deyab and F. Bentiss, Synthesis, characterization and comparative study of new functionalized imidazolium-based ionic liquids derivatives towards corrosion of C38 steel in molar hydrochloric acid, *Int. J. Electrochem. Sci.*, 2012, **7**(8), 6998–7015.

20 E. Berdimurodov, A. Kholikov, K. Akbarov, L. Guo, S. Kaya, K. P. Katin, D. K. Verma and M. Rbaa, Dagdag O: novel cucurbit[6]uril-based [3]rotaxane supramolecular ionic liquid as a green and excellent corrosion inhibitor for the chemical industry, *Colloids Surf., A*, 2022, **633**, 127837.

21 B. El-Haitout, R. Salghi, M. Chafiq, N. Elboughdiri, B. Hammouti, S. Fatimah, A. Chaouiki, J. Kang and Y. Gun

Ko, *J. Mol. Struct.*, 2025, **1322**(part 2), DOI: 10.1016/j.molstruc.2024.140520.

22 F. EL Hajjaji, R. Salim, M. Taleb, F. Benhiba, N. Rezki, D. S. Chauhan and M. A. Quraishi, Pyridinium-based ionic liquids as novel eco-friendly corrosion inhibitors for mild steel in molar hydrochloric acid: Experimental & computational approach, *Surf. Interfac.*, 2021, **22**, 100881.

23 R. Salim, A. Nahlé, F. El-Hajjaji, E. Ech-chihbi, F. Benhiba, F. El Kalai, N. Benchat, H. Oudda, A. Guenbour, M. Taleb, I. Warad and A. Zarrouk, Experimental, Density Functional Theory, and Dynamic Molecular Studies of Imidazopyridine Derivatives as Corrosion Inhibitors for C38 steel in Hydrochloric Acid, *Surf. Eng. Appl. Electrochem.*, 2021, **57**(2), 233.

24 A. Nahlé, R. Salim, F. El Hajjaji, M. R. Aouad, M. Messali, E. Ech-chihbi, B. Hammouti and M. Taleb, Novel triazole derivatives as ecological corrosion inhibitors for mild steel in 1.0 M HCl: experimental & theoretical approach, *RSC Adv.*, 2021, **11**(7), 4147–4162.

25 F. El-Hajjaji, E. Ech-chihbi, N. Rezki, F. Benhiba, M. Taleb, D. S. Chauhan and M. A. Quraishi, Electrochemical and theoretical insights on the adsorption and corrosion inhibition of novel pyridinium-derived ionic liquids for mild steel in 1 M HCl, *J. Mol. Liq.*, 2020, **314**, 113737.

26 A. Chaouiki, F. Hazmatulhaq, D. I. Han, A. H. Al-Moubaraki, M. Bakhouch and Y. G. Ko, Predicting the interaction between organic layer and metal substrate through DFTB and electrochemical approach for excellent corrosion protection, *J. Ind. Eng. Chem.*, 2022, **114**, 190.

27 A. Singh, K. R. Ansari, J. Haque, P. Dohare, H. Lgaz, R. Salghi and M. A. Quraishi, Effect of electron donating functional groups on corrosion inhibition of mild steel in hydrochloric acid: experimental and quantum chemical study, *J. Taiwan Inst. Chem. Eng.*, 2018, **82**, 233–251.

28 E. Ech-Chihbi, F. El Hajjaji, A. Titi, M. Messali, S. Kaya, G. Serdaroğlu, B. Hammouti and M. Taleb, Towards understanding the corrosion inhibition mechanism of green imidazolium-based ionic liquids for mild steel protection in acidic environments, *Indones. J. Sci.*, 2024, **9**(2), 395–420.

29 R. O. Medupin, K. O. Ukoba, K. O. Yoro and T. C. Jen, Sustainable approach for corrosion control in mild steel using plant-based inhibitors: A review, *Mater. Today Sustain.*, 2023, **22**, 100373.

30 F. El-Hajjaji, M. Messali, A. Aljuhani, M. R. Aouad, H. B. B. M. E. Chauhan D.S and M. A. Quraishi, Pyridazinium-based ionic liquids as novel and green corrosion inhibitors of carbon steel in acid medium: Electrochemical and molecular dynamics simulation studies, *J. Mol. Liq.*, 2018, **249**, 997–1008.